Aerosol Science & Technology

ISSN: 0278-6826 (Print) 1521-7388 (Online) Journal homepage: https://www.tandfonline.com/loi/uast20

Computational Fluid Dynamic Predictions and Experimental Results for Particle Deposition in an Airway Model

Michael J. Oldham

To cite this article: Michael J. Oldham (2000) Computational Fluid Dynamic Predictions and Experimental Results for Particle Deposition in an Airway Model, Aerosol Science & Technology, 32:1, 61-71, DOI: 10.1080/027868200303939

To link to this article: https://doi.org/10.1080/027868200303939

Published online: 30 Nov 2010.

Aerosol Science and Technology 32:61–71 (2000)

Published by Taylor and Francis
0278-6826/00/$12.00 + .00

Computational Fluid Dynamic Predictions and Experimental Results for Particle Deposition in an Airway Model

Michael J. Oldham, Robert F. Phalen, and Thomas Heistracher*

AIR POLLUTION HEALTH EFFECTS LABORATORY, DEPARTMENT OF COMMUNITY AND ENVIRONMENTAL MEDICINE, UNIVERSITY OF CALIFORNIA, IRVINE, CA 92697-1825 AND INSTITUTE OF PHYSICS AND BIOPHYSICS, UNIVERSITY OF SALZBURG, HELLBRUNNER STRASSE 34, A-5020 SALZBURG, AUSTRIA

ABSTRACT. An area identified as having a high priority by the National Research Council (NRC 1998) relating to health effects of exposure to urban particulate matter is the investigation of particle deposition patterns in potentially-susceptible subpopulations. A key task for risk assessment is development and refinement of mathematical models that predict local deposition patterns of inhaled particles in airways. Recently, computational fluid dynamic modeling (CFD) has provided the ability to predict local airflows and particle deposition patterns in various structures of the human respiratory tract. Although CFD results generally agree with available data from human studies, there is a need for experimental particle deposition investigations that provide more detailed comparisons with computed local patterns of particle deposition. Idealized 3-generation hollow tracheobronchial models based on the Weibel symmetric morphometry for airway lengths and diameters (generations 3–5) were constructed with physiologically-realistic bifurcations. Monodisperse fluorescent polystyrene latex particles (1 and 10 μm aerodynamic diameter) were deposited in these models at a steady inspiratory flow of 7.5 L/min (equivalent to heavy exertion with a tracheal flow of 60 L/min). The models were opened and the locations of deposited particles were mapped using fluorescence microscopy. The particle deposition predictions using CFD for 10 μm particles correlated well with those found experimentally. CFD predictions were not available for the 1 μm diameter case, but the experimental results for such particles are presented.

* Corresponding author

INTRODUCTION

In recent years there has been interest in identifying research needs regarding the issue of human health effects of urban particulate matter (EPA 1998; Phalen and Lee 1998; NRC 1998). In its review, the Committee on Research Priorities for Airborne Particulate Matter of the National Research Council listed 10 research topics that were classified as having the highest priority. One of these 10 areas was the investigation of deposition patterns in respiratory tracts of potentially susceptible individuals. A key task identified to accomplish this priority was the development and refinement of mathematical models for predicting regional and local deposition in subpopulations such as elderly people and individuals with lung diseases. The advent of computational fluid dynamic modeling (CFD) of particle deposition in airway structures has the potential to provide predictions for the amount and rate of particle deposition in airways of virtually any specified structure. CFD has been used to study airflow and inhaled particle deposition in laboratory animals (Morgan et al. 1991; Kimbell et al. 1993; Cohen Hubal et al. 1996) and humans. Although CFD has been used to predict particle deposition in various regions of the human respiratory tract, no experimental bench-top particle deposition data obtained using the actual airway geometry used in CFD predictions are available for comparison. Such a comparison would enable evaluation of overall deposition efficiency and local patterns, as well as provide insight into accuracy of modeled deposition mechanisms in CFD. Detailed comparisons of experimental local particle deposition patterns with CFD predicted deposition patterns are needed to evaluate and provide guidance to CFD efforts.

Several investigators have utilized CFD to study particle deposition in various three-dimensional human tracheobronchial airway bifurcation models (Gradón and Orlicki 1990; Balásházy and Hofmann 1993a,b; Kinsara et al. 1993; Asgharian and Anjilvel 1994; Heistracher and Hofmann 1995, 1997). Each investigation has utilized a unique geometry, especially in the transition zone (proximal to the bifurcation) and bifurcation-connecting airway structure, so some of the anatomical models used are better approximations of actual lung anatomy than are others. Kinsara et al. (1993) used circular airways with a steep taper between airways of different sizes. Asgharian and Anjilvel (1994) used square channels and a linear extrapolation to define shapes of the bifurcation region for their geometry. In contrast, Gradón and Orlicki (1990) used the data of Horsfield and Cumming (1967) to design a more realistic bifurcation in order to calculate deposition fluxes. Balásházy and Hofmann (1993a,b) explored a range of bifurcations through use of both a "narrow" and a "wide" transition zone model; however, the carinal ridge of these 2 anatomical models were identical. The major difference between these 2 models is the shape of the transition from parent to daughter tubes. Subsequent work by Heistracher and Hofmann (1995) utilized the morphometric work of Horsfield et al. (1971) and Hammersley and Olson (1992) to construct a more realistic bifurcation that completely defines the airway bifurcation mathematically. These anatomical models were labeled PRB (physiologically realistic bifurcation) models. Subsequently, their work was extended to a double bifurcation model with 3 airway generations (Heistracher and Hofmann 1997). This PRB double bifurcation model was chosen for our experimental particle deposition work since it was completely defined mathematically, enabling construction of a hollow model, and because it appears to be the most realistic

CFD bifurcation model that has yet been described.

MATERIALS AND METHODS

Hollow Tracheobronchial Model

The airway anatomy used in this study (PRB model of Heistracher and Hofmann 1995) is shown in Figure 1. This 3 generation anatomical model was based upon the symmetric Weibel (1963) adult human tracheobronchial airway descriptions for generations 3–5. The airway dimensions that were used are shown in Table 1. A complete description of the airway surface (including the important bifurcation region) can be found in the appendix to the Heistracher and Hofmann (1995) publication.

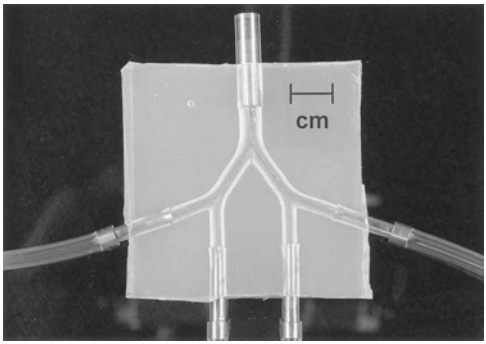

FIGURE 1. Hollow silicone rubber (Sylgard®, Dow, Midland, MI) PRB model with brass connectors used in this study.

TABLE 1. Airway morphometry of hollow tracheobronchial models.

Generation	Airway Diameter (mm)	Airway Length (mm)	Branch Angle (degrees)
1	5.6	11.0	0
2	4.5	9.2	35
3	3.6	7.7	35

Note: Details regarding complete mathematical definition of these bifurcation zones can be found in Heistracher and Hofmann (1995, 1997).

Solid epoxy airway models were produced from the CFD airway anatomy data file using sterolithography by a commercial firm (Scion Technologies, Santa Clarita, CA). The photo-curing epoxy selected for the solid models was Somos^{TM} 6110 (E. I. du Pont de Nemours and Company, New Castle, DE) because of its potential for resolving fine detail. The solid epoxy models, having all airway centers in a plane, were potted in silicone rubber (Dow, Midland, MI). After curing of the silicone, solid epoxy models were removed from the silicone rubber through slits. The slits were carefully sealed with the same type of silicone rubber. Hollow tracheobronchial airway model outlets were fitted with brass connector tubes having internal diameters closely matching the airway outside diameters. Particle deposition experiments were conducted at a steady inspiratory airflow rate of 7.5 L/min, which simulated a tracheal flow rate of 60 L/min and represented a state of heavy exertion. Prior to each run, airflow was calibrated with a 14.5 liter bell-type spirometer (Warren E. Collins Inc., Braintree, MA). For each particle deposition run, hollow tracheobronchial models were oriented horizontally (90° to the gravity vector).

Particle Generation and Deposition

Two sizes of monodisperse fluorescent polystyrene latex particles were used: 0.96 μm and 9.7 μm (nominal geometrical diameters). The 0.96 μm particles were purchased from a commercial supplier (Duke Scientific, Palo Alto, CA) and had a density of 1.05 g/cm^3. The 9.7 μm particles were purchased from a another supplier (Interfacial Dynamics Corporation, Portland, OR) and had a density of 1.06 g/cm^3. The mass median aerodynamic diameter

(MMAD) was calculated using data provided by the suppliers (sizes were verified in our laboratory using light microscopy). Thus, the MMADs of particles used in this study were 0.98 μm (~ 1 μm) and 9.97 (~ 10 μm).

A Lovelace-type compressed air nebulizer (Raabe 1972; In-Tox Products, Albuquerque, NM) was used to generate the fluorescent aerosols. The nebulizer was modified for use with larger particles by removing the baffle and enlarging the air jet in the nebulizer stem (Oldham et al. 1997). For deposition of 1 μm particles, hollow tracheobronchial models were fitted into a port on a rodent nose-only exposure manifold (In-Tox Products, Albuquerque, NM). In order to avoid large losses associated with 10 μm particles in the nose-only exposure manifold, a separate aerosol generation and delivery system (a copper enclosure) was used for these experiments (Oldham et al. 1997). Aerosols were generated at a nebulizer pressure of 1.4×10^{-4} kg m^{-2} (20 psi) from 0.1% (by volume) aqueous suspensions of particles in distilled water. Both particle suspensions were prepared so that $< 10\%$ of the particles would be generated as multiplets (Raabe 1968). Aerosols were dried and diluted using a radial diluter that injected dry air (5% RH) into the air stream. The quantity of dry dilution air was 10 times the nebulizer output. The aerosol was discharged to Boltzmann equilibrium by passing through a ^{85}Kr discharger (Liu and Pui 1974). Aerosols were pulled by a vacuum pump through the hollow tracheobronchial models. Particles that did not deposit in the models were collected on a 25 mm diameter polycarbonate filter (Nucleopore Corporation, Pleasanton, CA, acquired by Corning) and were quantified by fluorescence microscopy. Because of the large quantity of 1 μm particles on the filter, direct microscopic counting was impossible. Particles were removed from the filter by sonication in distilled water and quantified using a cell-counting hemocytometer method (Bhalla 1997). Particle removal from the filter was verified as complete by scanning the entire filter using fluorescence microscopy. For 10 μm particles, the particles on the filter were less numerous, and they were counted using fluorescence microscopy.

After deposition of fluorescent monodisperse particles, a line in the plane of the airway center lines was marked on the outside of the hollow models. The models were subsequently sliced into approximately equal top and bottom halves along this line. Fluorescent particle counts in photographic microscope fields were determined using fluorescence microscopy. In order to quantify particle deposition, a coordinate system was superimposed upon each half (top and bottom) of the hollow tracheobronchial model. Each rectangular field was divided into 4 equal quadrants, and particles in each quadrant were counted by 2 individuals. Particle counts were accepted and photographed after complete agreement. The large number of particles required to define local deposition patterns precluded exact determination of each particle's location. Additionally, a lack of 1 to 1 correspondence between microscopically-counted particles vs. particles counted from photographs (including confocal microscope images) prevented a photographic determination of particle counts and locations. Depth of field, surface texture, and light reflections from the hollow tracheobronchial models provided artifacts on photographs that were not problematic during counts at the microscope. Due to the magnification required and length of time required for analysis for the 1 μm particle run, each half of the hollow model was cut into 3 pieces by bisecting the second generation airway.

CFD Modeling

CFD predictions were available only for the 10 μm diameter particle case. For comparison of experimental deposition patterns to CFD predictions, deposition data of Heistracher and Hofmann (1997) was analyzed. Briefly, these CFD predictions were obtained using a commercial CFD package (FIRE, AVL List GmbH, Graz, Austria). FIRE is a general purpose CFD package based upon the finite volume approach. Heistracher and Hofmann (1997) used the conjugate-gradient method with preconditioning and convergence acceleration for solution of the linear equation systems. The boundary conditions used in the CFD predictions included a parabolic velocity entrance profile with constant pressure boundary conditions at the model exits (ambient pressure of 1.0×10^5 Pa). With Reynolds numbers ranging from 1882 to 733, a k-epsilon turbulence model, with k being the turbulent kinetic energy and epsilon the turbulence dissipation rate, was used. Particle-wall interactions were modeled using a "prismatic" approach. When a spherical particle is moving on a straight line, the enveloping surface is a cylinder. In general, the pathways will be curved lines, which can be subdivided into straight sections. The cylindrical pieces of the pathway were approximated by prisms (e.g., with 8 or more edges), where the number of edges were selected via input parameters. This "prismatic" approach allowed for strict consideration of interception, which is important near significantly curved regions of the surface (in the vicinity of the carinal ridge). For the experimental work, entry flow, exit flow, and boundary conditions were similar, except that the entrance flow profile was probably not fully parabolic. From Figure 3 of Heistracher and Hofmann (1997), the particle deposition locations were reduced to the number of particles that would have been seen in the microscope fields used to examine the hollow tracheobronchial models.

RESULTS

The overall deposition efficiencies for 1 μm and 10 μm aerodynamic diameter particles in hollow tracheobronchial models were 0.01% and 81%, respectively. As expected, the larger particles exhibited less uniform deposition patterns, which are typical of inertial effects. A total of 4,614 1 μm particles were deposited, counted, and mapped to determine the deposition of the top (2a) and bottom (2b) halves (Figure 2). The shading scheme is shown in Figure 2c. A total of 2,316 10 μm particles were deposited, counted, and mapped to determine the deposition pattern (Figure 3). The CFD simulation had a total of 2000 particles entering the first airway with 1,616 particles depositing, resulting in a deposition efficiency of 81%. Because of the need to use connectors to attach the hollow model to aerosol generation and flow control tubing, a small length of entrance and exit airways modeled in CFD was not available for analysis experimentally. A total of 16 particles that deposited in the top of the entrance airway in the CFD simulation were excluded from this analysis since this area was covered with a connector, thus resulting in a revised overall deposition efficiency for the CFD prediction of 80%.

In both the 1 μm and 10 μm experimental results, a slight left to right asymmetry in particle deposition was detected. In both runs, slightly more particles were on the left side than the right side (the difference was about 2.5% of the total). Part of this difference may be a counting artifact due to the way the grid system was superimposed on the hollow tracheobronchial models. The difference in number of particles on the left versus right sides, which was

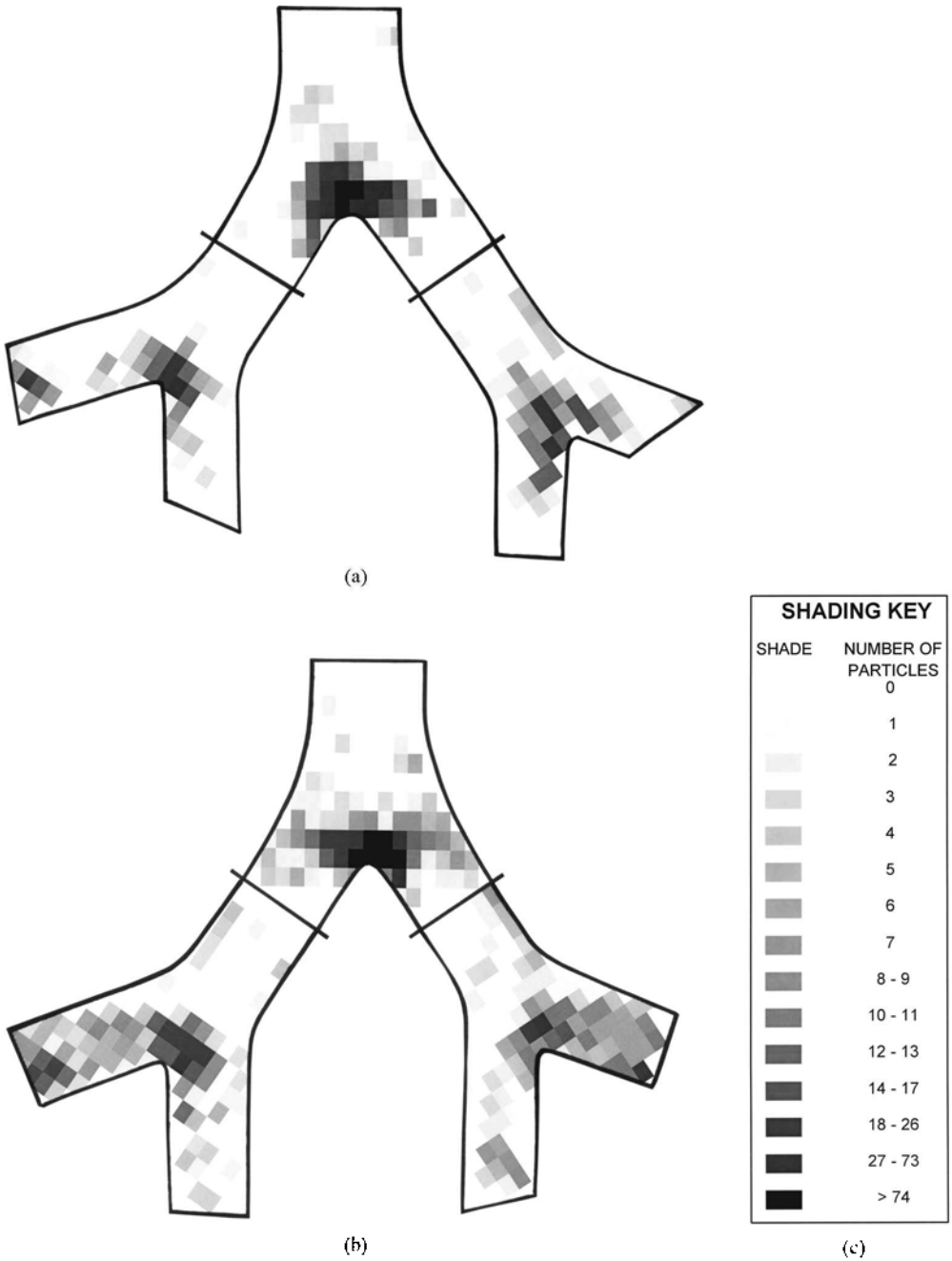

FIGURE 2. Deposition pattern for 1 μm MMAD monodisperse particles displayed as particle density per microscopic field for top (a) and bottom (b) halves of hollow PRB model: (c) shading scheme. Each rectangle represents a microscopic rectangular field of 1.4 mm × 0.95 mm.

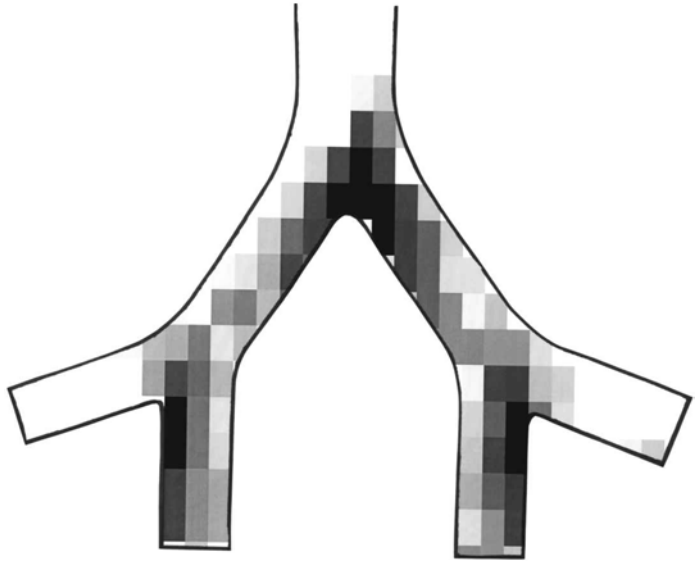

FIGURE 3. Deposition pattern for 10 μm MMAD monodisperse particles displayed as particle density per microscopic field for the entire hollow PRB model. Each rectangle represents a microscopic rectangular field of 2.05 mm × 1.4 mm. The shading scheme used is shown in Figure 2c.

judged to be accurate enough to compare with the CFD prediction, indicates that airflow distribution through the model was acceptably symmetric.

DISCUSSION

Although particles smaller than 10 μm in aerodynamic diameter are most relevant to environmental exposures, this test of CFD predictions used 10 μm particles because of the availability of predictions in an anatomical model that was relatively realistic and constructable using the steroliography process. Furthermore, 10 μm particles have small but finite deposition efficiencies in tracheobronchial airways of people. Using the particle deposition model of the National Council on Radiation Protection and Measurement (NCRP 1997), at near-resting ventilation an average nose-breathing adult will deposit about 6% of the total number of 10 μm particles inhaled (taking into account the inhalability, which is 71%). For mouth-breathing, the tracheobronchial deposition of 10 μm particles will be greater, due to lower deposition efficiencies for the mouth in comparison to the nose. The NCRP model predicts $< 3\%$ tracheobronchial deposition during nose breathing for 1 μm aerodynamic diameter particles, even though the nasal deposition is only 17% and the inhalability is 97%. If and when CFD predictions are available for 1 μm particles in the PRB model, our experiments for such particles can be used to test the predictions.

Figures 2 and 3 show that particle deposition patterns for 1 μm and 10 μm particles were consistent with deposition mechanisms (impaction, sedimentation, and diffusion) which are used in CFD predicted deposition. As would be expected for both particle sizes, enhanced deposition at bifurcations occurred, presumably due to impaction. Figure 4 shows a plot of cumula-

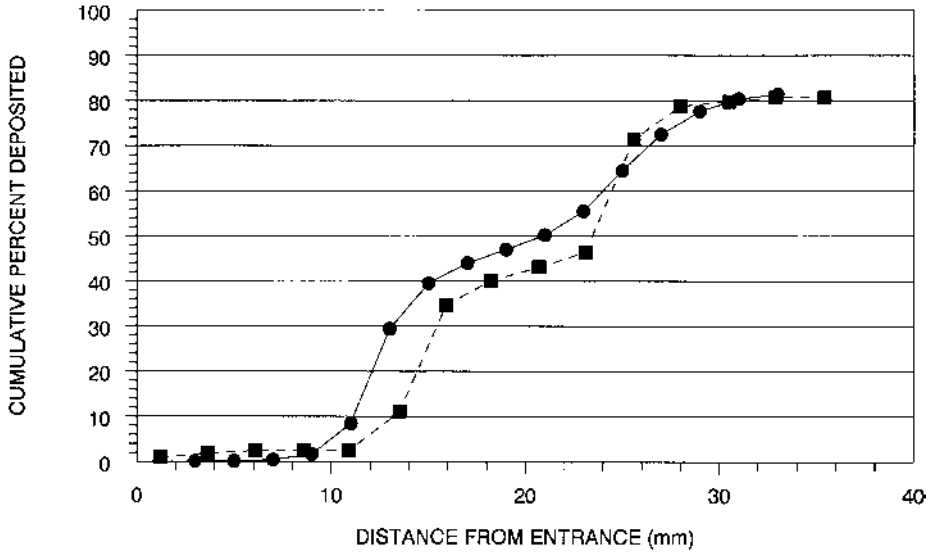

FIGURE 4. Cumulative percent deposition for 10 μm MMAD monodisperse particles plotted from the hollow model entrance to exits for both experimental data ● and CFD prediction ■.

tive percent deposition from the entrance to the exits of the hollow model for both experimental results and CFD prediction by Heistracher and Hofmann (1997) for 10 μm particles deposited at a flow rate of 7.5 L/min. This graph demonstrates the close agreement between experimental results and CFD predictions. Similar heavy deposition occurred at both proximal and distal bifurcations. The differences seen in this graph are more apparent when the local deposition pattern is viewed in the shading scheme used for the experimental data. Figure 5a shows the Heistracher and Hofmann (1997) CFD prediction for particle deposition pattern for 10 μm particles deposited at a flow rate of 7.5 L/min. In Figure 5b, this pattern has been converted to the identical shading scheme used for experimental data. The number of particles deposited were normalized to the number experimentally deposited. Similarities and differences in local deposition patterns can be seen from a comparison of Figures 3 and 5b. In addition to predicting heavy deposition at both proximal and distal bifurcations, both CFD predictions and experimental results showed a gradient of particle deposition from the outer airway wall to the inner airway wall in airways between proximal and distal bifurcations. Also, both CFD predicted and experimental results showed similar patterns of heavy deposition on the inside of one of the daughter airways and very little deposition on the corresponding side of the other daughter airway. In general, the experimental deposition pattern is not as concentrated in specific areas as CFD predictions. Additionally, CFD predicted a significant amount of deposition in the entrance region that was not observed in our experiment. This could be due to use of a brass connector in experiments to smoothly attach the model to the aerosol system. Additionally, the upstream effect of the carinal ridge to an initially parabolic flow profile might cause this deposition in the CFD prediction.

The agreement in overall deposition ef-

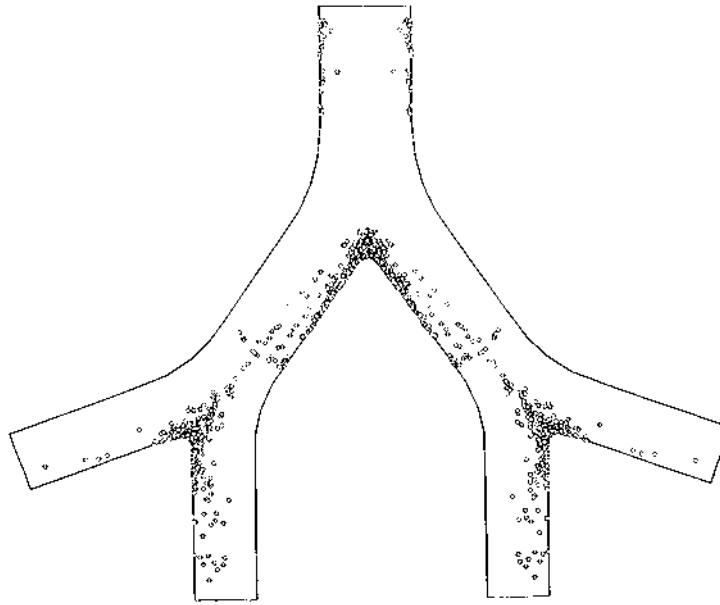

(a)

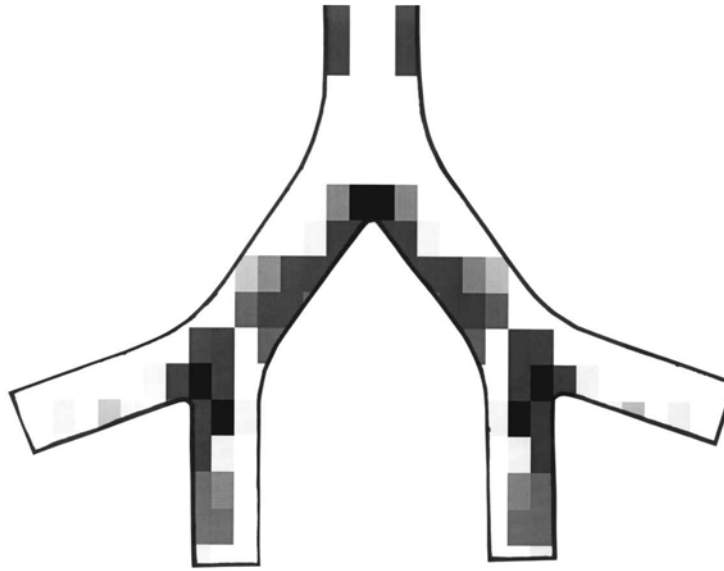

(b)

FIGURE 5. (a) 10 μm particle deposition pattern predicted by CFD; adapted from Heistracher and Hofmann (1997). (b) The same pattern converted to shaded fields as used in the microscopic analysis of experimental deposition in the hollow model.

ficiency and the similarity between local deposition patterns predicted by CFD and our experimental results indicates that CFD may be a viable tool for predicting particle deposition in hollow tracheobronchial models. The discrepancies in local deposition patterns point to the need to carefully examine both experimental artifacts (effects of charge, model surface roughness, etc.) and assumptions used in CFD predictions. Additional work will be required on more realistic airway geometries before particle deposition predictions from CFD can be confidently applied to human airways. However, the agreement between experimental and CFD results in this study is encouraging.

This research was supported by the National Heart, Lung, and Blood Institute (R01 HL39682) and the Tobacco-Related Disease Research Program (6LT-066). Dr. Phalen is a member of the University of California, Irvine, Center for Occupational and Environmental Health.

References

Asgharian, B., and Anjilvel, S. (1994). Inertial and Gravitational Deposition of Particles in a Square Cross Section Bifurcating Airway, *Aerosol Sci. Technol.* 20:177–193.

Balásházy, I., and Hofmann, W. (1993a). Particle Deposition in Airway Bifurcations–I. Inspiratory Flow, *J Aerosol Sci.* 24:745–772.

Balásházy, I., and Hofmann, W. (1993b). Particle Deposition in Airway Bifurcations–II. Expiratory Flow, *J Aerosol Sci.* 24:773–786.

Bhalla, D. K. (1997). Specialized Sampling Techniques. In *Methods in Inhalation Toxicology*, edited by R. F. Phalen. CRC Press, Boca Raton, FL, pp. 137–138.

Cohen Hubal, E. A., Kimbell, J. S., and Fedkiw, P. S. (1996). Incorporation of Nasal-Lining Mass-Transfer Resistance into a CFD Model for Prediction of Ozone Dosimetry in the Upper Respiratory Tract, *Inhal. Toxicol.* 8:831–857.

EPA, U.S. Environmental Protection Agency (1998). *Particulate Matter Research Needs for Human Health Risk Assessment to Support Future Reviews of the National Ambient Air Quality Standards for Particulate Matter*, EPA/600/R-97132F, U.S. Environmental Protection Agency, Research Triangle Park, NC.

Gradón, L., and Orlicki, D. (1990). Deposition of Inhaled Aerosol Particles in a Generation of the Tracheobronchial Tree, *J. Aerosol Sci.* 21:3–19.

Hammersley, J. R., and Olsen, D. E. (1992). Physical Models of the Smaller Pulmonary Airways, *J. Appl. Physiol.* 72:2402–2414.

Heistracher, T., and Hofmann, W. (1995). Physiologically Realistic Models of Bronchial Airway Bifurcations, *J. Aerosol Sci.* 26:497–509.

Heistracher, T., and Hofmann, W. (1997). Flow and Deposition Patterns in Successive Airway Bifurcations, *Ann. Occup. Hyg.* 41(Suppl. 1): 537–542.

Horsfield, K., and Cumming, G. (1967). Angles of Branching and Diameters of Branches in the Human Bronchial Tree, *Bull. Math. Biophys.* 29:245–259.

Horsfield, K., Dart, G., Olson, D. E., Filley, G. F., and Cumming, G. (1971). Models of the Human Bronchial Tree, *J. Appl. Physiol.* 31:207–217.

Kimbell, J. S., Gross, E. A., Joyner, D. R., Godo, M. N., and Morgan, K. T. (1993). Application of Computational Fluid Dynamics to Regional Dosimetry of Inhaled Chemicals in the Upper Respiratory Tract of the Rat, *Toxicol. Appl. Pharmacol.* 121:253–263.

Kinsara, A. A., Tompson, R. V., and Loyalka, S. K. (1993). Computational Flow and Aerosol Concentration Profiles in Lung Bifurcations, *Health Phys.* 64:13–22.

Liu, B. Y. H., and Pui, D. Y. H. (1974). Electrical Neutralization of Aerosols, *J Aerosol Sci.* 5:465–472.

Morgan, K. T., Kimbell, J. S., Monticello, T. M., Patra, A. L., and Fleishman, A. (1991). Studies of Inspiratory Airflow Patterns in the Nasal Passages of the F344 Rat and Rhesus Monkey Using Nasal Molds: Relevance to Formaldehyde Toxicity, *Toxicol. Appl. Pharmacol.* 110:223–240.

NCRP, National Council on Radiation Protection and Measurements (1997). *Deposition, Retention and Dosimetry of Inhaled Radioactive Substances*, National Council on Radiation Protection and Measurements, Bethesda, MD, pp. 50–68.

NRC, National Research Council (1998). *Research Priorities for Airborne Particulate Matter*, National Academy Press, Washington, D.C.

Oldham, M. J., Mannix, R. C., and Phalen, R. F. (1997). Deposition of Monodisperse Particles in Hollow Models Representing Adult and Child-Size Tracheobronchial Airways, *Health Phys.* 72:827–834.

Phalen, R. F., and Lee, J. S. (1998). Research Needs Relating to Health Effects of Exposure to Low Levels of Airborne Particulate Matter, *Appl. Occup. Environ. Hyg.* 13:352–355.

Raabe, O. G. (1968). The Dilution of Monodisperse Suspensions for Aerosolization, *Am. Ind. Hyg. Assoc. J.* 29:439–443.

Raabe, O. G. (1972). Operating Characteristics of Two Compressed Air Nebulizers used in Inhalation Experiments. In *Fission Product Inhalation Program Annual Report 1971–1972*, Inhalation Toxicology Research Institute, Albuquerque, NM, LF-45:1–6.

Weibel, E. R. (1963). *Morphometry of the Human Lung*, Springer, Berlin.

Received December 8, 1998; accepted March 29, 1999.